Iraqi Journal of Physics, 2025
https://doi.org/10.30723/ijp.v23i2.1369

Vol.23, No.2, PP. 64-79
P-ISSN: 2070-4003
E-ISSN: 2664-5548

Physical Properties and Microbial Effect of Zinc Oxide NPs Rapid Biosynthesis by Microwave Irradiation

Amenah Isam Al-Shammari[1] and Zainab J. Shanan[1*]
[1]*Department of Physics, College of Science for Women, University of Baghdad, Baghdad, Iraq*
[*]Corresponding author: Zainabjs_phys@csw.uobaghdad.edu.iq

Abstract

This study used the green method to synthesise zinc oxide nanoparticles by microwave irradiation, using plant extracts of tea, coffee, and rosemary separately and $Zn(NO_3)_2.6H_2O$; this method is considered eco-friendly, rapid, and cost-effective. The structural properties of prepared materials were investigated with an X-ray diffractometer (XRD), atomic force microscope (AFM), Fourier transform infrared (FTIR) spectroscope, and field emission scanning electron microscope (FESEM). Energy Dispersive X-ray (EDX) analysis was used to prove the presence of ZnO NPs. The electrical charge of the surface of nanomaterials was measured by Zeta potential, where 20 mV is adequate for ensuring physical stability. The three green extracts (tea, coffee, and rosemary) were 21.9, 14.7, and 15.5 mV, respectively. The shapes of the zinc oxide nanoparticles were irregular and agglomerated, and the average particle size was 59.96, 24.63, and 24.59 nm for the three extracts. Infrared spectroscopy using the Fourier transform (FT-IR) methods verified the presence of C=O, N-O, and C-H bonds; these results confirm the high reducing and capping capacity of ZnO NPs via biomolecules found in the plant extract. A UV-Vis spectrometer was used to study the light properties, and the energy gap was found to be 3.31, 3.26, and 3.35 eV for the tea, coffee, and rosemary extracts, respectively. Finally, ZnO NPs were used to inhibit the activity of many kinds of fungi and bacteria, both gram-positive and gram-negative. Studies have demonstrated their ability to penetrate the bacterial cell wall and halt the bacterial activity.

Article Info.

Keywords:
Biosynthesis, Microwave Irradiation, Plants Extract, SEM, Biological Activities.

Article history:
Received: Sep. 08,2024
Revised: Nov.26, 2024
Accepted:Dec.21, 2024
Published:Jun. 01,2025

1. Introduction

Nanoparticles are materials with a three-dimensional structure and vary in size from 1 to 100 nanometers. This substance consists of several atoms (molecules) that create various structures, including crystal, spherical, tubular, and amorphous forms [1]. They contain significant qualities in relation to their masses, particularly the ability to increase their surface area to volume ratio. This property is crucial as it enables their utilization in various creative and advanced fields (agricultural, food processing, cosmetics, medical treatment, and diagnostics) [2, 3]. Metal oxide nanomaterials, such as ZnO, CuO, TiO_2, and NiO, have garnered significant scientific interest due to their non-toxic nature, abundance, broad surface area, and exceptional chemical properties [4]. Furthermore, it has been shown that metal and metal oxide nanoparticles, such as copper, titanium and zinc oxides, and silver and gold metals, interact with one another. These compounds are among the best-known inorganic antibacterial agents [5]. One method that is both economical and kind to the environment is green production of nanoparticles. Green chemistry is important in nanotechnology through plant-mediated production of nanoparticles [6].

Recent trends in microwave-assisted oxide synthesis are becoming increasingly popular due to its environmentally benign nature, efficient heat transfer, and elevated reaction rate [7]. Compared to classical thermal procedures, the time required to create small particles is significantly reduced. Hence, this technology is highly regarded for its

ability to accelerate drug discovery and development processes [8]. Microwave chemistry relies on two fundamental principles: the dipolar and the electrical conductor mechanisms. The dipolar mechanism happens when a polar molecule aligns itself with the field in the presence of a high-frequency electric field. During this occurrence, the molecules emit sufficient thermal energy to propel the reaction in a forward direction. In the electrical conductor mechanism, the irradiated material acts as an electrical conductor, allowing ions and electrons (charge carriers) to move through the material due to the electric field. This movement results in polarization inside the material. The presence of induced currents and any electrical resistance result in the heating of the sample. The researchers have effectively showcased the implementation of this technique in the creation of nanostructures composed of silver, gold and platinum [9, 10]. The synthesis process determines the morphology of the nanoparticles. Nanorods, Nanoplates, Nanospheres, Hexagons, Tetrapods, and Nanoflowers are some examples of these nanostructures. Zinc oxide nanoparticles outperform other nanoparticles derived from the same element when it comes to killing gram-positive bacteria. Potentially harmful bacteria such as Salmonella, Staphylococcus aureus, and Escherichia coli pose a significant risk to the quality and safety of ready-to-eat foods and to be considered safe for human consumption [11].

The research aims to prepare zinc oxide nanoparticles in an environmentally friendly and inexpensive way with the help of microwave irradiation to reduce the synthesis time. Three plants were used in the preparation (tea, coffee, and rosemary). The properties of the prepared material were evaluated for application in measuring its biological activity on several types of bacteria and fungi.

2. Experimental Work

2.1. Biosynthesis of ZnO NPs using Plant Extracts (Tea, Coffee, and Rosemary)

To prepare green extracts, tea, coffee, and rosemary were acquired from the Iraqi market. 40 g of each was separately mixed well with 400 mL of distilled water, heated to eighty degrees Celsius and thereafter mixed well using the magnetic stirrer for 3, 1, and 2 h for tea, coffee, and rosemary, respectively. The watery mixture was then filtered, centrifuged at 6,000 rpm for fifteen minutes, and stored at 4 °C until needed.

To prepare the initial solution, 2.97 g of $Zn(NO_3)_2.6H_2O$ was combined with 100 mL of distilled water with applying low-heat for 5 minutes while using a magnetic stirring. Then, zinc nitrate solution and each of the (tea, coffee, rosemary) extracts were mixed with a 1:4 ratio on a magnetic stirrer for 5 minutes. Then the solution was exposed to microwave (SEVERIN,230V,50 Hz,1050 W, Made in China) irradiation at a power of 540 Watts for 5 minutes for coffee and 6-7 minutes for tea and rosemary. The solutions were centrifuged for 25 min, washed 5 times in distilled water and ethanol and filtered with filter paper until dry. The material was placed in the furnace (Electric Matsufuruda, Isu Seisakusho Co., Ltd., 100 V, 20 A.,1200°C MAXI, made in Japan) for 15 minutes at 800 ºC, and the final product was close to white in color, as shown in Fig. 1(b).

2. 2. Characterization for ZnO NPs

The ZnO NPs synthesized by the green method using tea, coffee and rosemary extracts were characterized with: XRD diffractometer (Aeris -Malvern Panalytical-Netherland); atomic force microscope (AFM) (NaioAFM 2022, Nanosurf-Switzerland) to examine the surface morphology; Fourrier-transform infrared spectrometer(FTIR) (1800-sgimadzu-Japan) to identify functional groups; Field emission scanning electron microscope (FE-SEM) (TESCAN MIRAIII-Czech) to provide information on the size and shape of the produced NPs, a spectral analysis was conducted to examine the distinctive peaks (EDX) to determine the microstructure and nanoscale parameters like

particle size and morphological-size; Ultraviolet-visible (UV–Vis) spectrophotometer(UV1900-shimadzu-Japan) to study the optical properties; and Zeta potential analyzer (Zetasizer Malvern Panalytica-Malvern) to determine the Zeta potential.

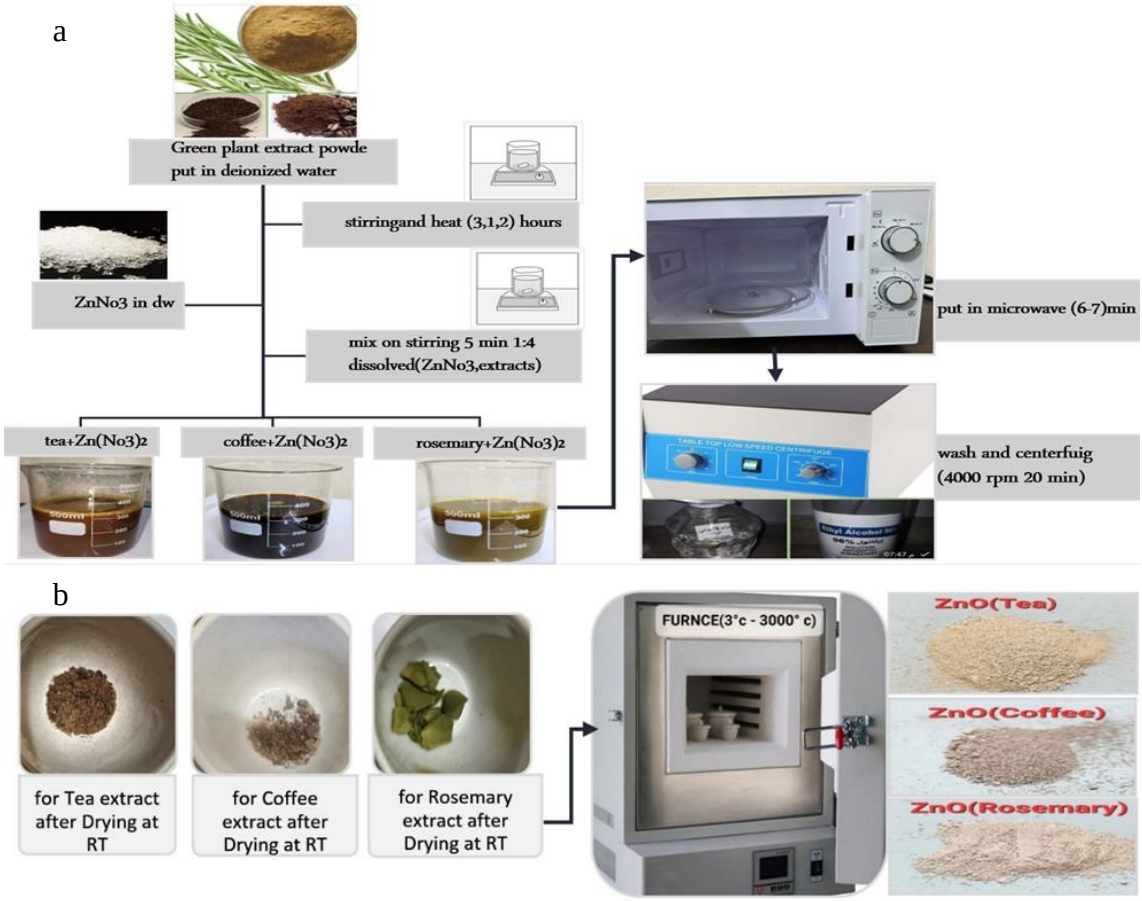

Figure* 1: *(a) Steps of preparing the plant extract and combine it with zinc nitrate to prepare zinc oxide NPs (b) Zinc oxide NPs powder synthesized by green synthesis.

2. 3. Biological efficacy method

Using the well diffusion method, an investigation was conducted to assess the antibacterial efficacy of zinc oxide nanoparticles on Mueller–Hinton agar (NHA) [12]. Gram-negative bacteria (Escherichia coli, Proteus mirabilis), gram-positive bacteria (Staphylococcus aureus, Bacillus Subtilis), and fungal isolates (Candida albicans) were tested. Under aseptic techniques, wells, each 6 mm in diameter, were cut out of the agar, which was contaminated with bacterial strains, and the wells were filled with 50% concentration of ZnO NPs. The plates were then incubated at 37ºC for 24 hours. After the incubation period, the diameters of the inhibitory zones were measured in millimeters.

3. Results and Discussion

3. 1. X-ray Diffraction Examination

XRD analysis was performed on the white powder following material preparation to assess its crystalline structure. The spectra were acquired using Cukα radiation at 40 kV and 40 mA. The XRD pattern was gathered at 2θ from 10-80 degrees. Fig. 2 displays the X-ray diffraction (XRD) patterns of zinc oxide NPs synthesized using the three green extracts (tea, coffee, and rosemary). The XRD patterns revealed several noticeable peaks appearing at 2θ angles of 31.7 º, 34.4 º, 36.2 º, 47.5 º, 56.5 º, 62.86 º,

6.3º, 67.96 º, 69.1 º, 72.55 º, and 76.99 º corresponding to Miller indices of 100, 002, 101, 102, 110, 103, 200, 112, 201, 004, and 202. Well-defined peaks with no impurities were observed. Similar results were obtained by other reported studies [11, 13-15]. The diffraction peaks were successfully matched to the hexagonal wurtzite crystal structure (JCPDS number 897102) [16]. In addition, the clear and focused diffraction peaks observed suggest that the produced ZnO NPs contain a high-quality crystalline structure using all three extracts. The average crystal size for zinc oxide NPs synthesized using tea, coffee, and rosemary extracts was determined using Scherer's formula, yielding values of 22.64 nm, 25.37 nm, and 24.88 nm, respectively

$$\text{Crystal size(D)} = \frac{K\lambda}{\beta\cos\theta} \quad (\mathbf{1})$$

where K is the form factor (0.94), λ is the X-ray wavelength of the incident radiation (0.154252) nm, β is the full width half maximum, and θ is the Bragg's angle [17]. While The length of the dislocation lines per unit volume of the crystal can be defined as the sample dislocation density (δ), which can be calculated as [18]

$$\delta = \frac{1}{D^2} \quad (\mathbf{2})$$

For the specified peak, strain rate (ε) was determined using the relation [18]:

$$\varepsilon = \frac{\beta\cos\theta}{4} \quad (\mathbf{3})$$

The dislocation density (δ), the crystal size values, and other structural properties of the biosynthesized zinc oxide nanoparticles with the microwave are displayed in Table 1. The variation in crystalline size and d_{hkl} values may be associated with different factors such as surface defects, strain, and dislocations. In other words, the decrease in crystalline size corresponds to an increase in the dislocation density values.

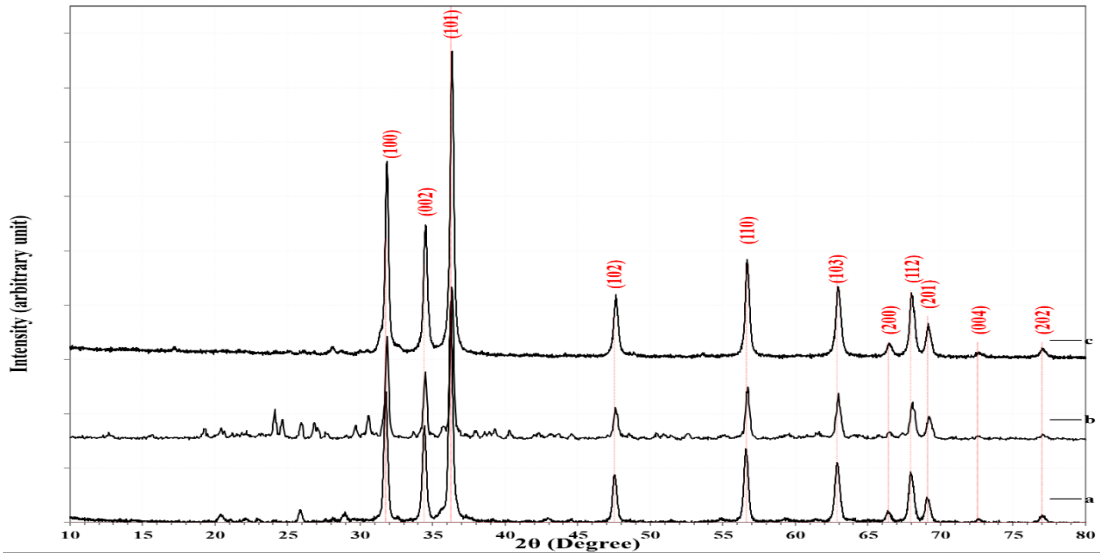

Figure 2: XRD patterns of microwave biosynthesized ZnO NPs by (a)tea, (b) coffee, and (c) rosemary extracts.

Table 1: Diffraction angle(2Θ), FWHM (β), planes distance (d), crystallite size(D), miller indices(hkl), dislocation density(δ), and strain (ε) of synthesized hexagonal ZnO NPs by (a)tea, (b)coffee, and (c)rosemary extracts.

(a)

2θ (Deg.)	**FWHM (Deg.)**	**d_{hkl} Exp.(Å)**	**D (nm)**	**(hkl)**	**d_{hkl} Std.(Å)**	**δ ×10^{15} (line/m^2)**	**ε**
31.7730	0.3546	2.8141	23.3	(100)	2.8137	1.84	0.0015
34.4208	0.3782	2.6034	22.0	(002)	2.6035	2.07	0.0016
36.2411	0.3546	2.4767	23.6	(101)	2.4754	1.80	0.0015
47.5414	0.3783	1.9110	23.0	(102)	1.9110	1.90	0.0015
56.5721	0.4019	1.6255	22.5	(110)	1.6245	1.98	0.0015
62.8605	0.3782	1.4772	24.6	(103)	1.4772	1.65	0.0014
66.3593	0.4492	1.4075	21.1	(200)	1.4069	2.24	0.0016
67.9669	0.4728	1.3781	20.3	(112)	1.3782	2.43	0.0017
69.1017	0.4492	1.3582	21.5	(201)	1.3582	2.17	0.0016
72.5532	0.3546	1.3019	27.8	(004)	1.3017	1.29	0.0012
76.9976	0.5201	1.2374	19.5	(202)	1.2377	2.62	0.0018

(b)

2θ (Deg.)	**FWHM (Deg.)**	**d_{hkl} Exp.(Å)**	**D (nm)**	**(hkl)**	**d_{hkl} Std.(Å)**	**δ ×10^{15} (line/m^2)**	**ε**
31.8663	0.2776	2.8060	29.8	(100)	2.8137	1.13	0.0012
34.4831	0.3171	2.5988	26.2	(002)	2.6035	1.45	0.0013
36.3070	0.2578	2.4724	32.4	(101)	2.4754	0.95	0.0011
47.5871	0.3370	1.9093	25.8	(102)	1.9110	1.51	0.0013
56.6865	0.3172	1.6225	28.5	(110)	1.6245	1.23	0.0012
62.9510	0.4163	1.4753	22.4	(103)	1.4772	2.00	0.0015
66.4996	0.4163	1.4049	22.8	(200)	1.4069	1.92	0.0015
68.0855	0.4163	1.3760	23.0	(112)	1.3782	1.88	0.0015
69.1759	0.3766	1.3569	25.6	(201)	1.3582	1.52	0.0014
72.5857	0.3965	1.3014	24.9	(004)	1.3017	1.62	0.0014
77.0065	0.5749	1.2373	17.7	(202)	1.2377	3.21	0.0020

(c)

2θ (Deg.)	**FWHM (Deg.)**	**d_{hkl} Exp.(Å)**	**D (nm)**	**(hkl)**	**d_{hkl} Std.(Å)**	**δ ×10^{15} (line/m^2)**	**ε**
31.8438	0.2749	2.8080	30.1	(100)	2.8137	1.11	0.0012
34.4905	0.3093	2.5983	26.9	(002)	2.6035	1.38	0.0013
36.3295	0.3094	2.4709	27.0	(101)	2.4754	1.37	0.0013
47.6209	0.3609	1.9080	24.1	(102)	1.9110	1.73	0.0014
56.6609	0.3609	1.6232	25.0	(110)	1.6245	1.60	0.0014
62.9511	0.4125	1.4753	22.6	(103)	1.4772	1.96	0.0015
66.4400	0.3953	1.4060	24.0	(200)	1.4069	1.73	0.0014
67.9696	0.3781	1.3781	25.3	(112)	1.3782	1.56	0.0014
69.1554	0.3781	1.3573	25.5	(201)	1.3582	1.53	0.0014
72.6442	0.4640	1.3005	21.3	(004)	1.3017	2.21	0.0016
77.0096	0.4641	1.2373	21.9	(202)	1.2377	2.09	0.0016

3. 2. Atomic Force Microscopy (AFM)

High-resolution surface topographic images from AFM were used to study surface morphology, as shown in Fig. 3. This widely used approach efficiently measures nanoparticle size and dispersion. The 3D scans showed a folded mountainous structure, maybe created by metal bonds or oxide layers [19]. AFM scanning was done by drying ZnO NPs on a clean glass plate. Average values of grain size were derived based on sample measurement location, as shown in Fig. 4, which depicts the surface shape of ZnO NPs generated with plant extracts. The grain size of ZnO NPs synthesized by (tea, coffee, and rosemary) extracts averaged 59.96, 24.63, and 24.59 nm, respectively. The shape of the nanoparticles was cohesive and semi-spherical. The results were close to those presented by Rajeshkumar et al. [20].

3. 3. Fourier Transform Infrared Examination

FTIR was used to assess the presence of phytochemicals on the surface of ZnO NPs. The results were analyzed and recorded in the frequency range 400-4000 $cm^{-1}$with 4 cm^{-1} resolution to determine the specific functional groups of botanical constituents that caused the reduction and stability of ZnO nanoparticles. The FTIR spectroscopy of ZnO nanoparticles synthesized by the three extracts (tea, coffee, and rosemary) with the assistance of microwave radiation is shown in Fig. 4. and Table 2. Strong peaks around 420.49 – 471.7 cm^{-1} referring to the Zn-O band in ZnO. These results agree with those of Mohammadian et al. [21] and Rini et al. [22]. As per research, the vibration bands are found between 2852.37–2927.5 cm^{-1} to (CH_2) [13, 23]. Also, the other peaks between 1052.49 –1066.03 cm^{-1} refer to C-O. These results are in agreement with other published results [21, 24, 25]. The peak at 1537.38 cm^{-1} corresponds to the stretching of C–H bonds, at 3419 - 3443 cm^{-1} represents the stretching of the O–H bonds. These results agree with other reported studies [21, 24, 26, 27]. The peak at 1687.67 cm^{-1} corresponds to H_2O [28].

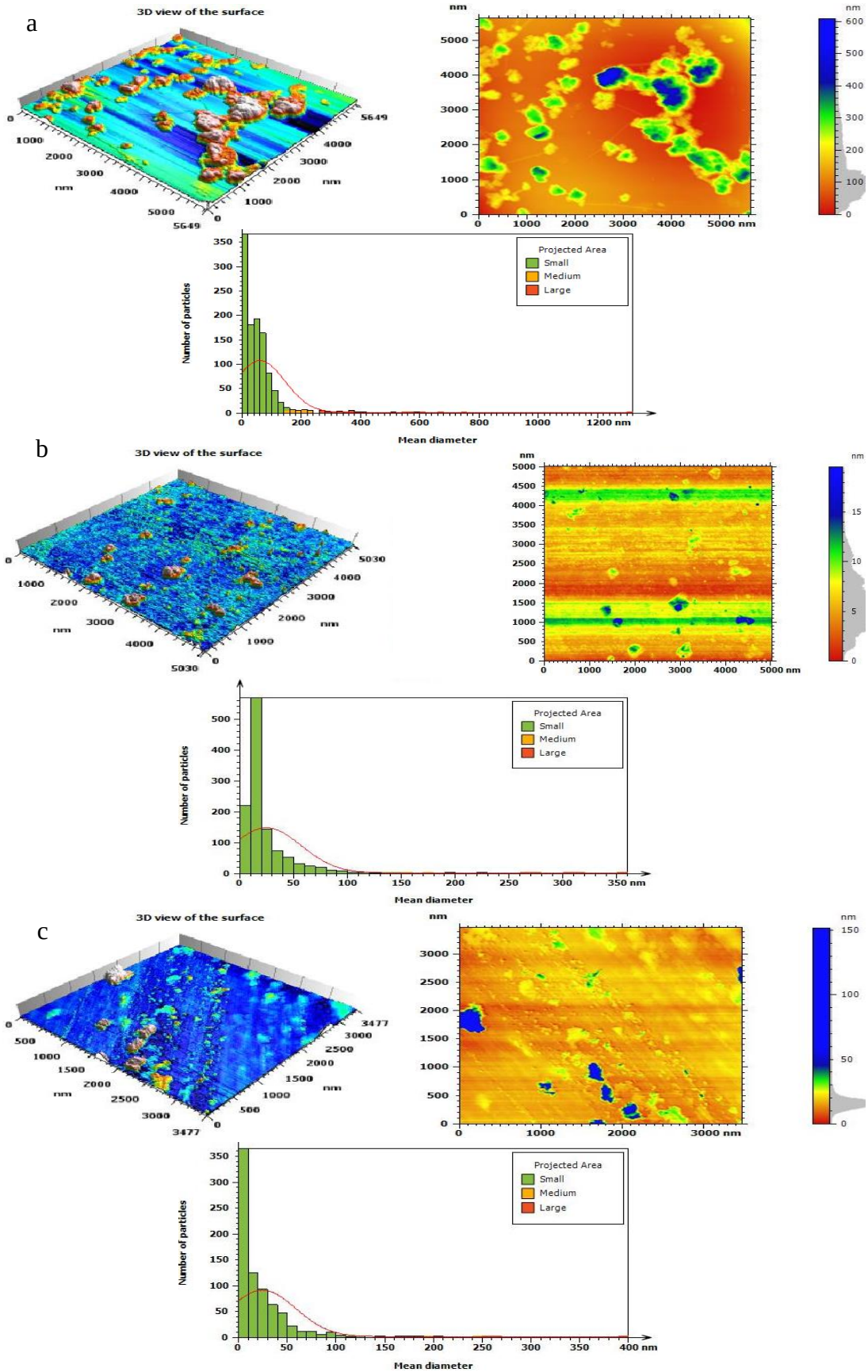

Figure 3: AFM images of zinc oxide NPs synthesized by: (a)tea, (b)coffee and (c)rosemary extracts.

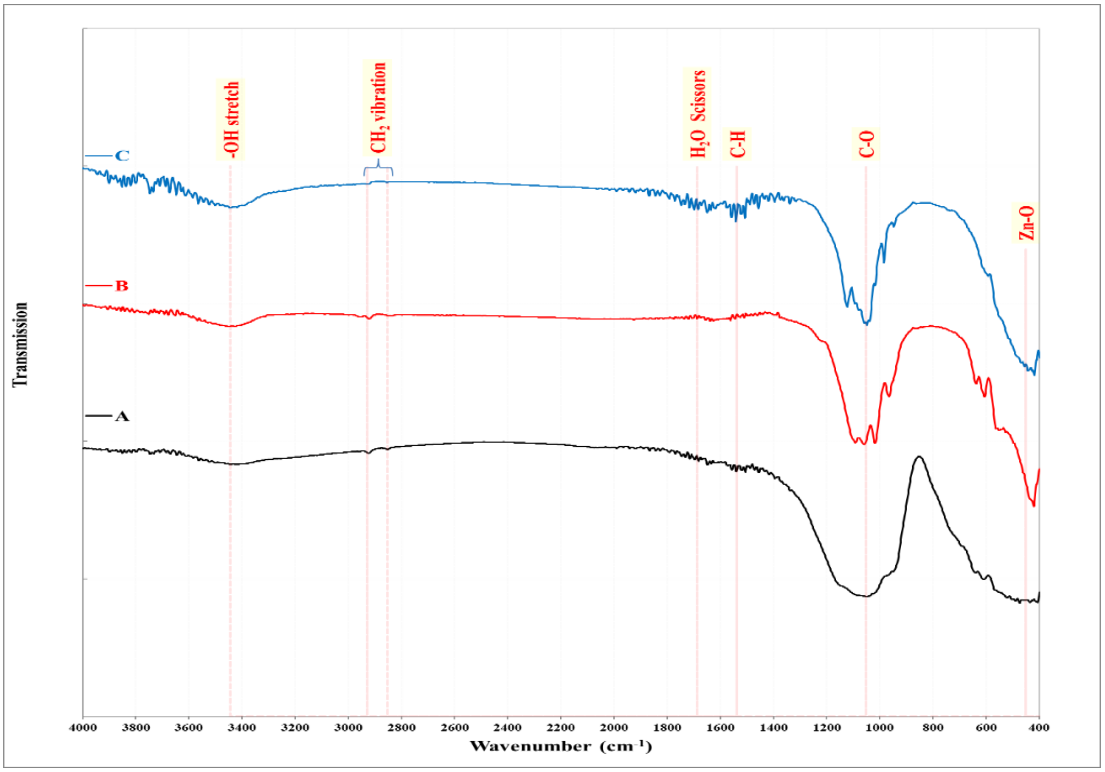

Figure 4: FTIR analysis for zinc Oxide nanoparticles synthesized with three different extracts: (A) tea, (B) coffee, and (C) rosemary.

Table 2: FTIR analysis for ZnO NPs synthesized by (A) tea, (B) coffee, and (D) rosemary extracts.

Band Type	A	B	C
O-H stretch	3419.35	3446.68	3443.26
CH2	2924.10 2852.37	2920.68 -	2927.51 -
H_2O Scissors	-	-	1687.67
C-H	-	-	1537.38
C-O	1066.03	1076.28	1052.37
Zn-O	471.73	420.49	420.49

3. 4. Field Emission Scanning Electron Microscopy (FESEM)

The produced ZnO NPs shape and atomic ratio were examined using filed emission scanning electron microscopy. The FESEM images of ZnO NPs generated using tea, coffee, and rosemary extracts with microwave irradiation at magnification 1 μm and 500 nm are shown in Fig. 5. It was observed from the figure that the ZnO NPs agglomerated into irregular shapes. The morphology of nanoparticles has a pivotal impact on their effectiveness against infections. Due to their ability to readily infiltrate the cell wall of pathogens, spherical nanoparticles are highly effective in their antibacterial effect [29]. ZnO NPs show modest aggregation, typical of green nanoparticles. Due to their increased surface area and strong attraction, biosynthetic nanoparticles aggregate or agglomerate [30]. The stability and aggregation of NPs are significantly impacted by ecological factors. During creation, nanoparticles adhere to one another and spontaneously form asymmetrical clusters [31]. Optimizing nanoparticle manipulation requires calibrating growth factors to achieve the desired size and shape. The growth factors are plant extract or biomass concentration, salt concentration, growth or reaction time, temperature, and solution pH [26]. This result was close to other reported studies [11, 32, 33].

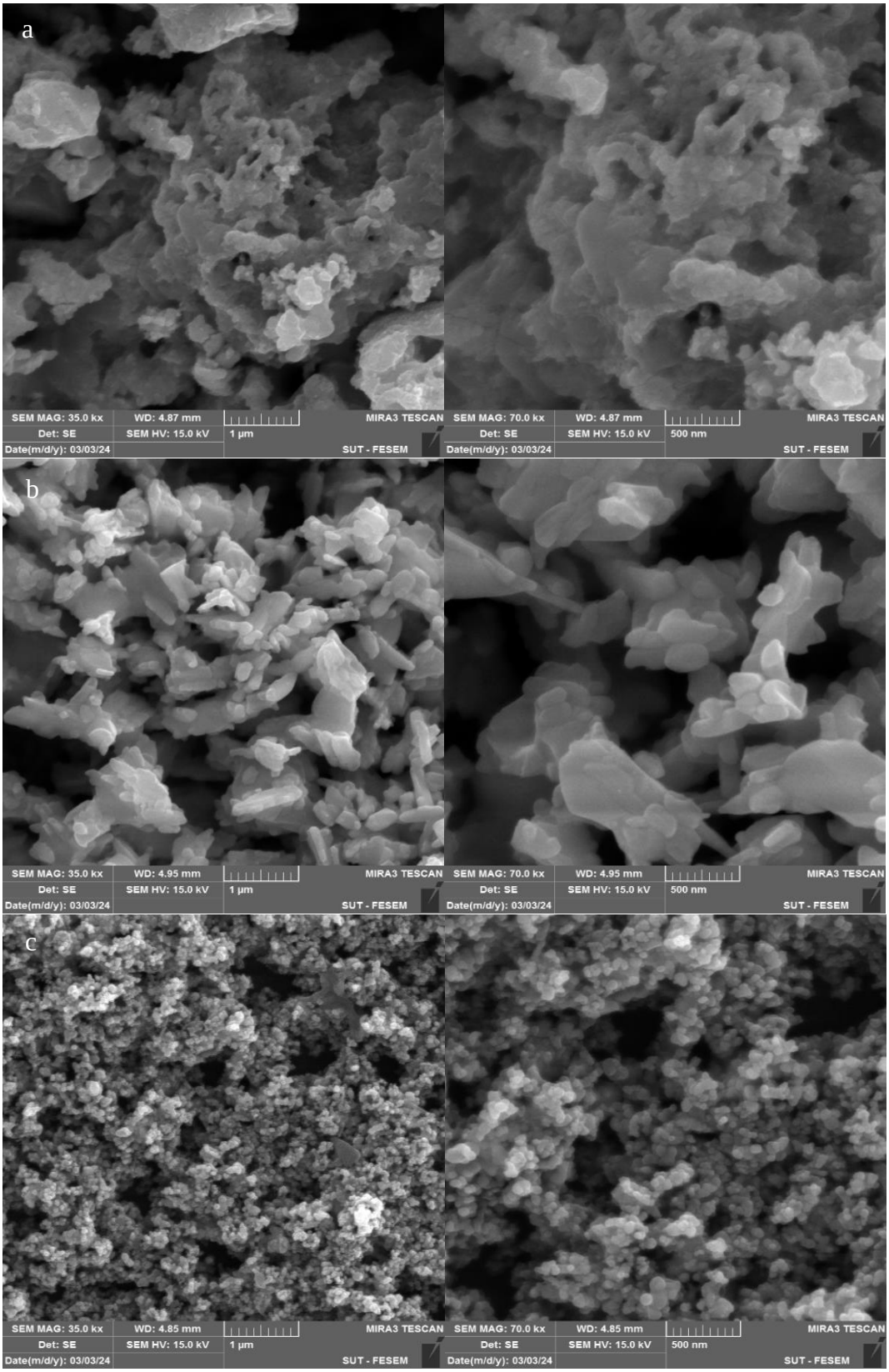

Figure 5: FESEM images of zinc oxide NPs synthesized by (a)tea, (b)coffee, and (c)rosemary extracts.

3. 5. Energy Dispersive X-ray (EDX)

Energy dispersive X-ray (EDX) analysis was conducted to examine the characteristics of ZnO NPs in more detail, as shown in Fig. 6. The presence of ZnO NPs

biosynthesized by (tea, coffee, and rosemary) extracts assisted by microwave radiation was verified using EDX analysis and examining its constituent elements. Zinc, oxygen, and gold existed in all the samples. The EDX spectra showed two strong zinc peaks and one oxygen peak. Fig.6(a) demonstrates the EDX spectrum of the ZnO NPs synthesized with tea extract; the data revealed the percentages of Zn of (76.38%) and O of (23.6%), where Zn peaks were at (1.1 and 8.6) keV while oxygen at 0.51 keV. Fig.6(b) shows the EDX spectrum of the ZnO NPs synthesized with coffee extract revealing the percentages of Zn (78.13%) and O (21.87%), while the peaks for zinc were at (1.1, 8.6) keV, and oxygen at 0.5 keV, Fig.6(c) demonstrates the EDX spectrum of the ZnO NPs synthesized with rosemary extract, where Zn peaks were at (1.1 and 8.6) keV, while O at 0.5 keV, with Zn percentages of (77.27%) and O of (22.73%). The peaks and data obtained agree with previous works [24-26, 28].

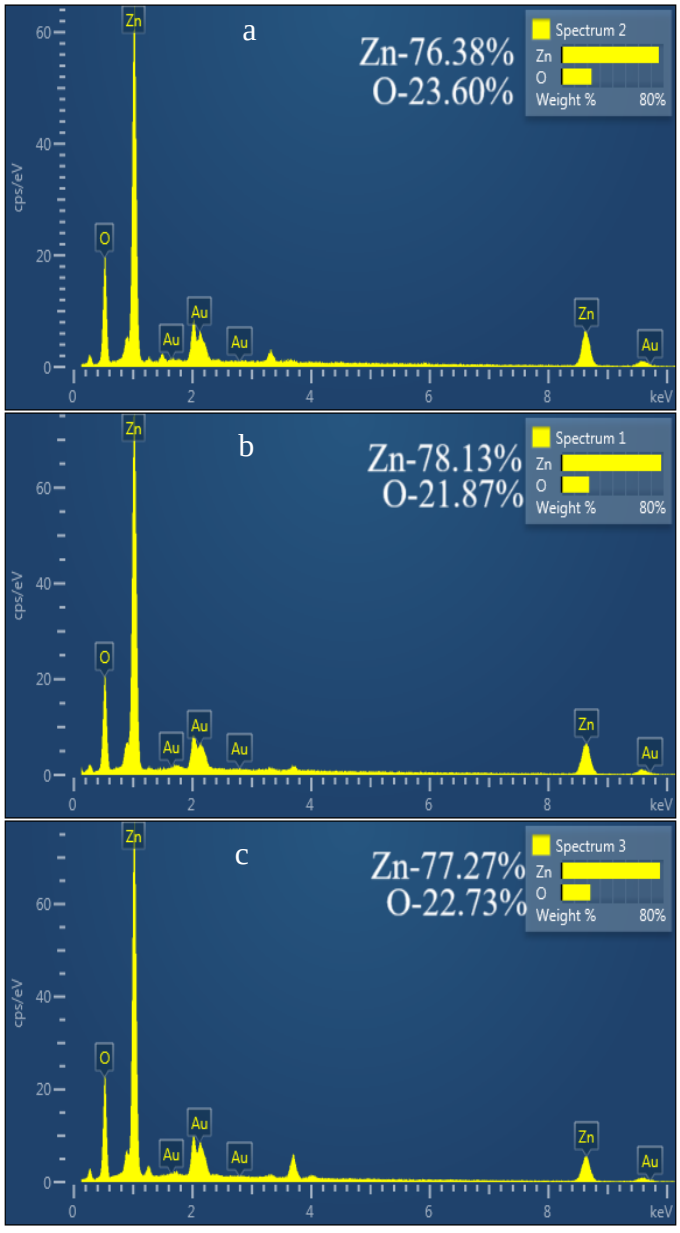

Figure 6: EDX for zinc oxide NPs synthesized by (a)tea, (b)coffee, and (c)rosemary extracts.

3. 6. Optical Examination

The reduction of metal ions and the formation of nanoparticles are represented by a peak absorption that is correlated with the surface Plasmon resonance (SPR) and gathers oscillations of conduction band electrons in reaction with electromagnetic waves [26]. Surface Plasmon resonance absorption bands are created when the free electrons in metal nanoparticles undergo recombination modifications and resonate with light waves [34]. The optical absorption spectra of ZnO NPs prepared with the three extracts (Tea, Coffee, and Rosemary) are depicted in Fig. 7. The measurement was conducted at room temperature. The spectra displayed distinct peaks at wavelengths of 370, 380, and 374 m, characteristic of ZnO nanoparticles for tea, coffee, and rosemary extracts, respectively, due to the SPR band of NPs. These phytochemicals are highly capable of stabilizing metal ions in the nanoscale dimension and reducing them, for being antioxidants and free of toxic substances. The presence of a distinct peak indicated the formation of ZnO nanoparticles with a uniform size distribution; by way of generalization, the highest absorption peak for ZnO nanoparticles falls within the range of 300 to 380 nm [26]. Since NPs' optical characteristics depend on their size, shape, aggregation, and componentry, they can be characterized utilizing the UV–Vis spectrum [35]. Results demonstrated that the energy band gaps for ZnO NPs synthesized by tea, coffee, and rosemary extracts were (3.31, 3.26, and 3.35) eV, respectively, as calculated according to the following formula:

$$\mathrm{E} = \frac{\mathrm{hc}}{\lambda m_{ax}} \qquad (\mathbf{4})$$

where h= (6.626×10^{-34} Js) represents the Planck constant, c = (3×10^{8} m/s) represents the speed of light, E represents the band-gap energy, and $\lambda_{max\ x}$ represents the maximum absorption [36].

It was noted that the band gap energy of the synthesized nanomaterials was consistently greater than that of their micron-sized counterparts across all sample groups. Low-dimensional crystallites' quantum mechanical phenomena cause nanomaterial band gap broadening. In these length scales, the energy levels overlap and become quantized, resulting in an expansion of the materials' band gap [37]. Also, particle size and configuration may cause the absorption peak to shift. However, this causes a wide ZnO particle size distribution. Decreasing the size of nanoparticles leads to an increase in the energy gap [18]. The results are close to other reported studies [21, 26, 27, 38-40].

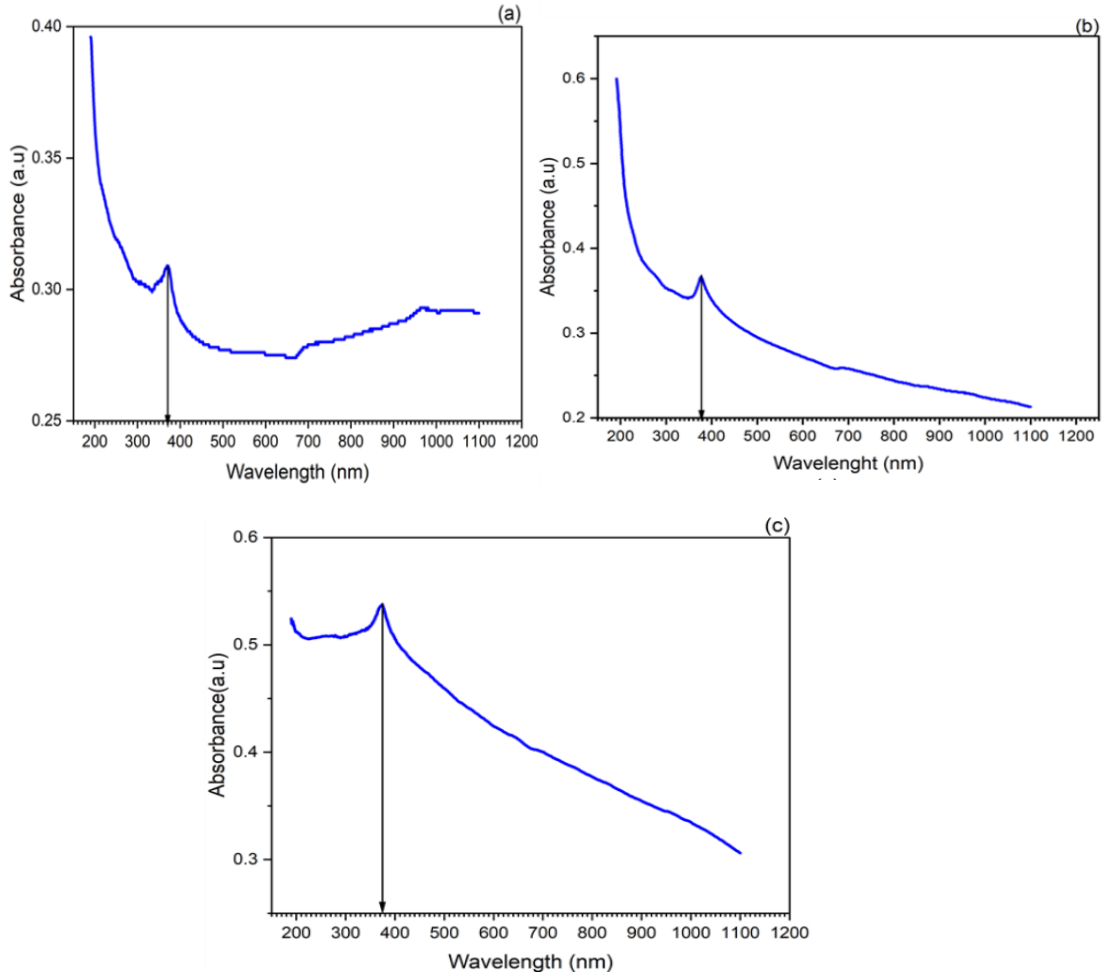

Figure 7: Absorption curves as a function of wavelength of microwave biosynthesized ZnO NPs by (a)tea, (b) coffee, and (c) rosemary extracts.

3. 7. Zeta potential (ZP) determination

Zeta potential is an essential tool for quantifying the electric charge of the surface of nanomaterials [41]. Zeta potential measures electrostatic repulsion between particles of the same charge in a dispersion. A high zeta potential guarantees stability for tiny molecules and particles, preventing aggregation in solutions or dispersions [42]. The parameter ZP is quite advantageous in forecasting the stability of dispersions including solid lipid nanoparticles. According to the literature, zeta potential values greater than 30 mV are beneficial. Physical stability is achieved when voltages exceed 60 mV. The temporary physical stability is 20 millivolts, with acceptable values ranging from -5 to +5, indicating rapid aggregation. However, this is not true for high molecular weight stabilizers, which work primarily through steric stabilization. In this instance, a zeta potential of 20 mV or less is adequate for ensuring physical stability. Before the examination, ZnO nanoparticles were dispersed in water and thoroughly mixed to assess their stability [43]. The measurements of the material appeared as in Fig. 8. The ZP values for the biosynthesized ZnO NPs by the three extracts (tea, coffee, and rosemary) were (21.9, 14.7 ,15.5) mV, respectively.

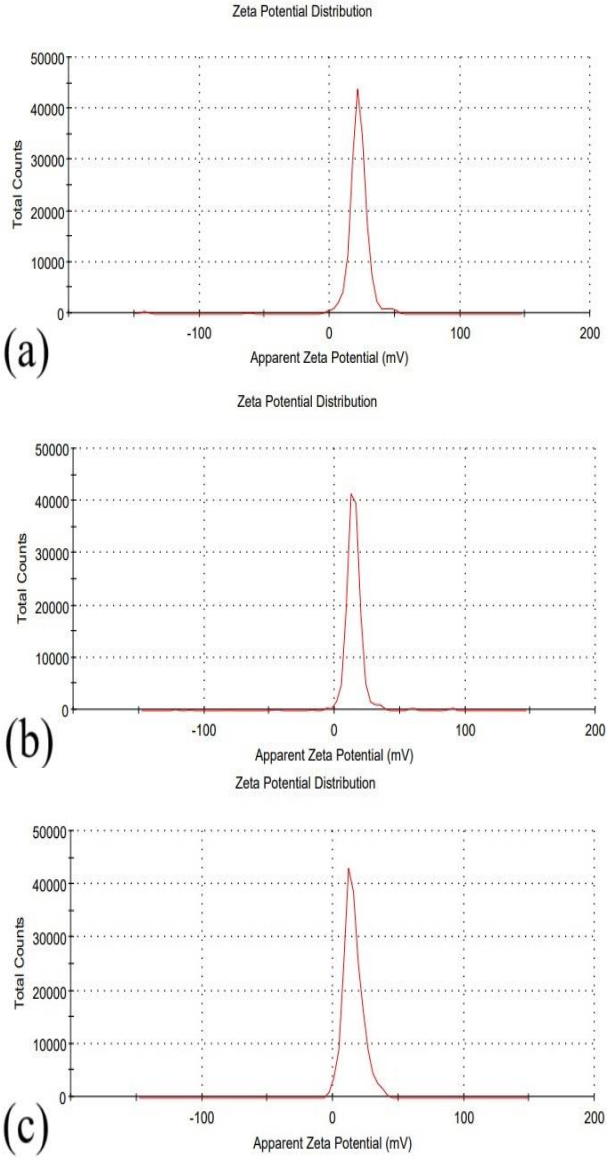

Figure 8: The zeta potential of zinc Oxide nanoparticles synthesized using the extracts of (a)tea, (b)coffee, and (c)rosemary.

3. 8. Antibacterial results

Three processes normally explain bacteria-NP interactions: the first forms highly active hydroxyls and the second deposits NPs on bacteria. Finally, NPs accumulate in the cytoplasm or periplasmic region of bacterium cells, disrupting cellular processes and membrane organization [39]. ZnO NPs were manufactured utilizing extracts derived from tea, coffee, and rosemary. The bacteria used in the study were shown to be susceptible to the quantity of nanoparticles that were formed; nanoparticles' antibacterial activity is a size dependent ability, and the property improves with the reduction of particle size. Table 3 displays the measurements of the inhibition zone of bacterial growth [20, 32]. ZnO NPs impede bacterial growth in numerous ways. These processes worked similarly efficiently against gram-positive (Staphylococcus aureus, Bacillus Subtilis), gram-negative bacteria (Proteus mirabilis, Escherichia coli) and Candida albicans, except for zinc oxide nanoparticles synthesized by coffee extract, which did not provide any activity against bacterial E. coli, as shown in Fig. 9. ZnO NPs inhibited E. coli at an inhibition

zone of 12.15 mm, whereas conventional medicines had a range of 15–20 mm inhibition zone. The inhibition zone against Staphylococcus aureus for ZnO NPs was 15-18 mm and this result was close to that of Rad et al. [40]. While The activity against B. subtilis was good, as evidenced by a zone of inhibition measuring between 19 and 21 mm, when compared to the positive control Tetracyclin, which displayed an inhibition zone of 28.50 mm [11, 25, 32]. The best nano ZnO was prepared using tea and rosemary extracts. The best results were in rosemary. but between coffee and tea, the proportions were varying in preference depending on the type of bacteria.

Table 3: Bacterial pathogen-fighting capabilities by ZnO nanoparticles.

	Zone of inhibition (mm)				
Samples ZnO NPs	**S. aureus (+)**	**B. Subtilus (+)**	**E. coli (-)**	**proteus mirabilis (-)**	**C. albicans**
1-Tea	15	19	12	21	11
2-Coffee	11	20	0	9	10
3-Rosemary	18	21	15	19	11

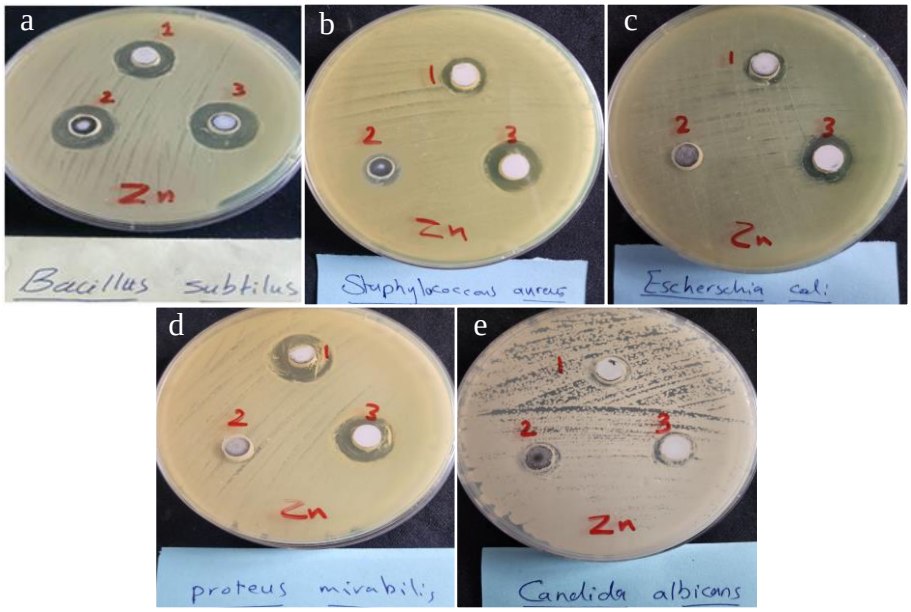

Figure 9: Zones of inhibition for antibacterial and fungal infections activity created by* ZnO Nps *(a) Bacillus subtilus, (b) staphylococcus aureus, (c) Escherichia coli, (d) Proteus mirabilis and (e) Candida albicans.

4. Conclusions

The process of ZnO NPs biosynthesis using microwave radiation by plant extracts (tea leaves, coffee, rosemary) was carried out successfully. The important role of microwave radiation has been proven in reducing the energy consumed, effort expended, and high prices by reducing the preparation time of the required material and protecting it from exposure to changes in the environment surrounding the material. The main advantages of microwave-assisted synthesis are purity from pollution, speed, efficiency, reduced work effort, substantially accelerated reaction rate, high yield, cost-effectiveness, and concentrating the radiation energy directly without dispersion. It was concluded from XRD tests that the average crystal size of zinc oxide NPs was that the prepared material was well crystallised and the size of the crystals was within the nanoscale range. The FTIR test revealed that the plant extracts (tea, coffee, and rosemary) contained most of the functional groups that aided in reducing zinc oxide nanoparticles. The agglomeration and aggregation of the material were observed from the field emission scanning electron microscope (FESEM) images, and the zeta potential results confirmed this. UV and

visible measurements revealed direct energy gaps for all the prepared samples. Finally, it was found that all the prepared samples were inhibitory to gram-positive and gram-negative bacteria and fungi; however, the samples prepared from rosemary and tea extracts gave the best results in terms of properties and application.

Acknowledgements

The cooperation of the Nano Lab, Department of Physics, College of Science for Women, University of Baghdad appreciated.

Conflict of interest

Authors declare that they have no conflict of interest.

References

1. S. Abel, J. L. Tesfaye, R. Shanmugam, L. P. Dwarampudi, G. Lamessa, N. Nagaprasad, M. Benti, and R. Krishnaraj, J. Nanomat. **2021**, 3413350 (2021). DOI: 10.1155/2021/3413350.
2. Z. J. Shanan, S. K. Shanshool, H. F. Al-Taay, N. K. Abdalameer, and S. M. Hadi, Int. J. Nanosci. **21**, 2250020 (2022). DOI: 10.1142/S0219581X2250020X.
3. D. Letchumanan, S. P. M. Sok, S. Ibrahim, N. H. Nagoor, and N. M. Arshad, Biomolecules **11**, 564 (2021). DOI: 10.3390/biom11040564.
4. Z. J. Shanan, S. M. Hadi, and S. K. Shanshool, Baghdad Science Journal, **15**, 211, (2018). DOI: 10.21123/bsj.2018.15.2.0211.
5. I. Hussain, N. B. Singh, A. Singh, H. Singh, and S. C. Singh, Biotech. Lett. **38**, 545 (2016). DOI: 10.1007/s10529-015-2026-7.
6. S. K. Shanshool and Z. J. Shanan, Int. J. Nanosci. **22**, 2350030 (2023). DOI: 10.1142/S0219581X23500308.
7. A. Verma, R. Dwivedi, R. Prasad, and K. S. Bartwal, J. Nanopart. **2013**, 737831 (2013). DOI: 10.1155/2013/737831.
8. F. Mavandadi and Å. Pilotti, Drug Dis. Today **11**, 165 (2006). DOI: 10.1016/S1359-6446(05)03695-0.
9. M. G. R. Priya, B. Raj, and T. Rashmi, European J. Biomed. Pharmaceut. Sci. **7**, 691 (2020).
10. C. O. Kappe, Angew. Chem. Int. Ed. **43**, 6250 (2004). DOI: 10.1002/anie.200400655.
11. Z. J. Shanan, N. K. Abdalameer, and H. M. J. Ali, Int. J. Nanosci. **21**, 2250017 (2022). DOI: 10.1142/S0219581X2250017X.
12. M. Balouiri, M. Sadiki, and S. K. Ibnsouda, J. Pharmaceut. Analy. **6**, 71 (2016). DOI: 10.1016/j.jpha.2015.11.005.
13. T. Al-Garni, N. A.Y. Abduh, A. Al-Kahtani, and A. Aouissi, Preprints **2021**, 2021040038 (2021). DOI: 10.20944/preprints202104.0038.v1.
14. R. Al-Gaashani, S. Radiman, N. Tabet, and A. R. Daud, Mat. Chem. Phys. **125**, 846 (2011). DOI: 10.1016/j.matchemphys.2010.09.038.
15. T. Prakash, R. Jayaprakash, G. Neri, and S. Kumar, J. Nanopart. **2013**, 274894 (2013). DOI: 10.1155/2013/274894.
16. B. Bulcha, J. Leta Tesfaye, D. Anatol, R. Shanmugam, L. P. Dwarampudi, N. Nagaprasad, V. L. N. Bhargavi, and R. Krishnaraj, J. Nanomat. **2021**, 8617290 (2021). DOI: 10.1155/2021/8617290.
17. M. Ali, J. El Nady, S. Ebrahim, and M. Soliman, Opt. Mat. **86**, 545 (2018). DOI: 10.1016/j.optmat.2018.10.058.
18. N. K. Bhoi, H. Singh, and S. Pratap, J. Inst. Eng. India Ser. C **101**, 407 (2020). DOI: 10.1007/s40032-019-00542-w.
19. P. Karpagavinayagam and C. Vedhi, Vacuum **160**, 286 (2019). DOI: 10.1016/j.vacuum.2018.11.043.
20. S. Rajeshkumar, R. P. Parameswari, D. Sandhiya, K. A. Al-Ghanim, M. Nicoletti, and M. Govindarajan, Molecules **28**, 2818 (2023). DOI: 10.3390/molecules28062818.
21. M. Mohammadian, Z. Es'haghi, and S. Hooshmand, J. Nanomed. Res. **7**, 00175 (2018). DOI: 10.15406/jnmr.2018.07.00175.
22. A. S. Rini, Y. Rati, and S. W. Maisita, J. Phys.: Conf. Ser. **2049**, 012069 (2021). DOI: 10.1088/1742-6596/2049/1/012069.
23. S. Sudha and A. Mary Saral, Mater. Res. Express **10**, 125401 (2023). DOI: 10.1088/2053-1591/ad02e0.
24. U. L. Ifeanyichukwu, O. E. Fayemi, and C. N. Ateba, Molecules **25**, 4521 (2020). DOI: 10.3390/molecules25194521.

25. K. K. P. Kumar, N. D. Dinesh, and S. K. Murari, Int. J. Nanopart. **11**, 239 (2019). DOI: 10.1504/IJNP.2019.102624.
26. A. A. Barzinjy and H. H. Azeez, SN Appl. Sci. **2**, 991 (2020). DOI: 10.1007/s42452-020-2813-1.
27. F. Rahman, M. A. Majed Patwary, M. A. Bakar Siddique, M. S. Bashar, M. A. Haque, B. Akter, R. Rashid, M. A. Haque, and A. K. M. Royhan Uddin, Roy. Soci. Open Sci. **9**, 220858 (2022). DOI: 10.1098/rsos.220858.
28. B. Naiel, M. Fawzy, M. W. A. Halmy, and A. E. D. Mahmoud, Sci. Rep. **12**, 20370 (2022). DOI: 10.1038/s41598-022-24805-2.
29. B. Wiley, Y. Sun, B. Mayers, and Y. Xia, Chem. A European J. **11**, 454 (2005). DOI: 10.1002/chem.200400927.
30. M. Sundrarajan, S. Ambika, and K. Bharathi, Adv. Powd. Tech. **26**, 1294 (2015). DOI: 10.1016/j.apt.2015.07.001.
31. H. Agarwal, S. Venkat Kumar, and S. Rajeshkumar, Res. Effici. Tech. **3**, 406 (2017). DOI: 10.1016/j.reffit.2017.03.002.
32. K. R. Raghupathi, R. T. Koodali, and A. C. Manna, Langmuir **27**, 4020 (2011). DOI: 10.1021/la104825u.
33. P. Sutradhar, M. Debbarma, and M. Saha, Synth. React. Inorg. Met. Org. Nano-Met. Chem. **46**, 1622 (2016). DOI: 10.1080/15533174.2015.1137035.
34. A. Sachdeva, S. Singh, and P. K. Singh, Mat. Today Proce. **34**, 649 (2021). DOI: 10.1016/j.matpr.2020.03.150.
35. X. Wang and Y. Cao, J. Indus. Eng. Chem. **82**, 324 (2020). DOI: 10.1016/j.jiec.2019.10.030.
36. R. A. Hayder and Z. J. Shanan, Int. J. Nanosci. **21**, 2250050 (2022). DOI: 10.1142/S0219581X22500508.
37. N. Kamarulzaman, M. F. Kasim, and R. Rusdi, Nanoscale Res. Lett. **10**, 346 (2015). DOI: 10.1186/s11671-015-1034-9.
38. K. R. Ahammed, M. Ashaduzzaman, S. C. Paul, M. R. Nath, S. Bhowmik, O. Saha, M. M. Rahaman, S. Bhowmik, and T. D. Aka, SN Appl. Sci. **2**, 955 (2020). DOI: 10.1007/s42452-020-2762-8.
39. M. J. Haque, M. M. Bellah, M. R. Hassan, and S. Rahman, Nano Ex. **1**, 010007 (2020). DOI: 10.1088/2632-959X/ab7a43.
40. S. S. Rad, A. M. Sani, and S. Mohseni, Micro. Pathogen. **131**, 239 (2019). DOI: 10.1016/j.micpath.2019.04.022.
41. A. F. Ismail, K. C. Khulbe, and T. Matsuura, *Reverse Osmosis* (Amsterdam, Netherlands, Elsevier, 2019).
42. S. Thomas, R. Thomas, A. K. Zachariah, and R. K. Mishra, *Thermal and Rheological Measurement Techniques for Nanomaterials Characterization* (Amsterdam, Netherlands, Elsevier, 2017).
43. B. Hilweh, H. Soliman, and M. M. Alajlani, Wor. J. Pharm. Pharmaceut. Sci. **12**, 43 (2023). DOI: 10.20959/wjpps20237-25214.

الخواص الفيزيائية والتأثير الميكروبي للتخليق الحيوي السريع لجسيمات أكسيد الزنك النانوية بواسطة تشعيع الميكروويف

امنة عصام الشمري[1] و زينب جاسم شنان[1]

[1] *قسم الفيزياء، كلية العلوم للبنات، جامعة بغداد، بغداد، العراق*

الخلاصة

في هذه الدراسة تم استخدام الطريقة الخضراء لتصنيع جزيئات أكسيد الزنك النانوية عن طريق تشعيع الميكروويف، وذلك باستخدام المستخلصات النباتية لكل من (الشاي والقهوة وإكليل الجبل) بشكل منفصل و$Zn(NO_3)_2.6H_2O$، والتي تعتبر سهلة الاستخدام وسريعة وفعالة من حيث التكلفة. تم دراسة الخواص التركيبية للمواد المحضرة بواسطة تقنية تحليل حيود الأشعة السينية، مجهر القوة الذرية، تحويل فورييه للتحليل الطيفي للأشعة تحت الحمراء والمجهر الإلكتروني لمسح انبعاث المجال .ولمزيد من التفاصيل، تم استخدام تحليل الأشعة السينية المشتتة للطاقة لإثبات وجود أكسيد الزنك. تم قياس الشحنة الكهربائية لسطح المواد النانوية بواسطة جهد زيتا حيث أن 20 ملي فولت كافية لضمان الاستقرار الجسدي. وبالنسبة للمستخلصات الخضراء الثلاثة (الشاي والقهوة وإكليل الجبل) فقد كانت (21.9، 14.7، 15.5) ملي فولت على التوالي. كانت أشكال جسيمات أكسيد الزنك النانوية غير منتظمة ومتكتلة، وكان متوسط حجم الجسيمات 59.96، 24.63، و24.59 نانومتر. أثبت التحليل الطيفي للأشعة تحت الحمراء باستخدام طرق تحويل فورييه (FT-IR) وجود روابط C=O وN-O وC-H، وتؤكد هذه النتائج قدرة الاختزال والتغطية العالية لأكسيد الزنك NPs عبر الجزيئات الحيوية الموجودة في المستخلص النباتي. بالإضافة إلى ذلك تم استخدام مطياف الأشعة فوق البنفسجية والمرئية (UV-Vis)لفحص الخصائص البصرية، حيث تم تحديد فجوة الطاقة بقيمها (3.31، 3.26، 3.35) فولت عند استخدام مستخلصات الشاي والقهوة وإكليل الجبل على التوالي. أخيرًا، تم استخدام ZnO NPs لتثبيط نشاط العديد من أنواع الفطريات والبكتيريا، سواء إيجابية الجرام أو سلبية الجرام، وقد ثبت أنها يمكن أن تدخل جدار الخلية البكتيرية وتوقف عمل البكتيريا.

الكلمات المفتاحية: التخليق الحيوي، تشعيع الميكروويف، المستخلصات النباتية، المجهر الالكتروني الماسح، الأنشطة البيولوجية.